Internal oxidation of In and Cd impurities in silver

W. Segeth, D. O. Boerma, L. Niesen, and P. J. M. Smulders
Laboratorium voor Algemene Natuurkunde and Materials Science Center, Groningen University, Westersingel 34, NL-9718 CM Groningen, The Netherlands
(Received 29 June 1988)

Internal oxidation of indium and cadmium implanted in silver single crystals has been studied by time-differential perturbed angular correlation (TDPAC) as well as by nuclear-reaction analysis (NRA) with the $^{18}O(p,\alpha)^{15}N$ reaction. Oxidation at 550 K results in the formation of the so-called indium-oxygen 2*a* complexes, as observed with ^{111}In TDPAC. The main axis of the axially symmetric electric field gradient (EFG) of this complex is pointing in a ⟨100⟩ crystallographic direction. The NRA measurements show that two oxygen atoms are trapped, at near-interstitial sites, by each indium atom. After subsequent annealing above 700 K, the geometry of the 2*a* complexes has changed and the so-called 2*b* complexes are formed. The asymmetry parameter of the EFG equals $\eta=0.8(2)$ with the *z* and *y* axes pointing in ⟨100⟩ directions. Again, two oxygen atoms are trapped at each indium atom, but with 40% of the oxygen atoms shifted into near-substitutional sites. The other 60% are located at "random" sites. This change in electronic and geometric structure occurring at the $2a \rightarrow 2b$ transition might be due to trapping of thermally activated vacancies by the 2*a* complexes. Subsequent annealing above 873 K results in the agglomeration of the 2*b* complexes into In_2O_3 precipitates. Annealing at 1050 K leads to dissociation of these precipitates. Internal oxidation of very dilute cadmium in silver single crystals below 700 K leads to the formation of cadmium-oxygen complexes with the TDPAC characteristics of the InO_2 2*a* complexes.

I. INTRODUCTION

The first hyperfine-interaction study of internal oxidation of radioactive impurities in silver was done with ^{119}Sn Mössbauer spectroscopy (MS). Using this probe, MS is mainly sensitive to the isomer shift, which is determined by the electron density at the nucleus. Pasquevich *et al.*[1] made the first ^{111}In time-differential perturbed-angular-correlation (TDPAC) measurements on internal oxidation of In*Ag* alloys. The ^{111}In TDPAC method is mainly sensitive to the quadrupole interaction and therefore gives information complementary to the Mössbauer measurements.

Oxidation of very dilute ^{111}In*Ag* alloys at oxidation temperatures $T_{ox} < 700$ K gives rise to a rather broad distribution of quadrupole frequencies in the ^{111}In (TDPAC) spectrum with an average value $\nu_Q = 60-65$ MHz,[2,3] caused by the formation of the isolated indium-oxygen complexes. Uhrmacher and co-workers[3] have denoted this component as the 2*a* complex. With increasing oxidation temperature, the average frequency shifts gradually to a maximum value of $\nu_Q = 95-100$ MHz around 600 K.[3-5] This new component is denoted as the 2*b* complex. Oxidation above 775 K results in the formation of In_2O_3 precipitates. These are recognized by two well-defined frequencies in the TDPAC spectrum. A strong dependence of the growth of the precipitates on the indium concentration is observed.[2,4] The most recent work of this kind was done by Uhrmacher and co-workers,[6,7] who studied the process of internal oxidation of indium in the presence of radiation defects.

In this paper we present the results of combined TDPAC and nuclear reaction analysis (NRA) or channeling measurements on internal oxidation of dissolved indium in silver crystals. A microscopic model for the 2*a* and 2*b* complexes is proposed. In addition, the results of internal-oxidation experiments on dilute ^{111m}Cd in silver are presented. With this isotope, the same intermediate level is used for TDPAC as in the case of ^{111}In.

II. MECHANISM OF INTERNAL OXIDATION

A. Two-step oxidation model

The classical model to describe the mechanism of preferential oxidation of dilute non-noble-metal impurities in a noble metal was developed by Wagner.[8] According to this model, the oxygen enters the metal at the surface and diffuses through a layer, containing already oxidized impurities, to the inward-moving oxidation front, where the oxygen atoms get immediately trapped at the nonoxidized or partly oxidized impurities.

We developed a two-step oxidation model, an extended version of Wagner's model, that takes into account the dissociation energy of the partly oxidized impurities.[9] For the impurities indium and antimony, we always found that two oxygen atoms are trapped by these impurities to form stable complexes. At low oxidation temperatures the mobility of the impurities can be neglected and the diffusion of oxygen atoms in a field of traps can be described as

$$\frac{\partial C_O}{\partial t} = D_O \frac{\partial^2 C_O}{\partial z^2} - S_B - S_{BO} \,. \tag{1}$$

The terms S_B and S_{BO} describe the trapping at a nonoxidized *B* atom and a *BO* complex, respectively,

$$S_B = k_B^A C_O C_B - k_{BO}^D C_{BO} \quad (B + O \leftrightarrows BO) , \tag{2}$$

$$S_{BO} = k_{BO}^A C_O C_{BO} \quad (BO + O \rightarrow BO_2) , \tag{3}$$

where k^A and k^D are the association and dissociation constants. The time development of the different complexes is described by the rate equations

$$\frac{\partial C_B}{\partial t} = -S_B , \tag{4a}$$

$$\frac{\partial C_{BO}}{\partial t} = S_B - S_{BO} , \tag{4b}$$

and

$$\frac{\partial C_{BO_2}}{\partial t} = S_{BO} . \tag{4c}$$

The boundary conditions are given by

$$C_O(0,t) = C_O^s , \tag{5a}$$

$$C_O(z \rightarrow \infty, t) = 0 , \tag{5b}$$

$$C_B(z,0) = C_B^i(z) , \tag{5c}$$

$$C_{BO}(z,0) = 0 , \tag{5d}$$

and

$$C_{BO_2}(z,0) = 0 . \tag{5e}$$

With Eqs. (1)–(5) the two-step oxidation model is completely described. We have solved these equations numerically using the subroutine D03PGF of the mathematical library NAG.

B. Diffusion parameters

In the absence of strain, the diffusion of oxygen in silver can be described as a random walk:

$$D_O = D_O^0 \exp\left[\frac{-E_O^m}{kT}\right] \quad \text{with } D_O^0 = \tfrac{1}{6}\nu\lambda^2 , \tag{6}$$

where E_O^m is the migration energy, ν is the Debye frequency of the oxygen, and λ is the length of the jump vector. The most recent value of $D_O^0 = 3.66 \times 10^{-3}$ cm^2/s is determined from oxygen degassing experiments by Eichenauer and Müller[10] in the temperature range from 673 to 1173 K. They found $E_O^m = 0.48$ eV for the migration energy.

The oxygen concentration at the surface was determined in the same experiment as

$$C_O^s = 2.8 \times 10^{-3}\sqrt{p} \exp\left[\frac{-H_O^s}{kT}\right] , \tag{7}$$

with a solution enthalpy of $H_O^s = 0.51$ eV and the oxygen pressure p in mbar.

The reaction constant k_B^A is given by

$$k_B^A = Z\nu \exp\left[\frac{-E_O^m}{kT}\right] . \tag{8}$$

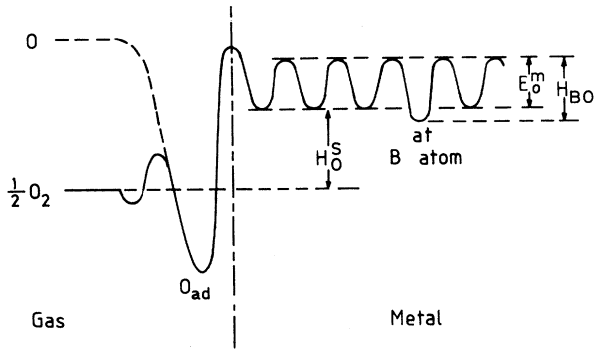

FIG. 1. Potential-energy diagram for the silver-oxygen system with non-noble-metal impurities as used in the two-step oxidation model.

The geometric factor Z is the number of new nearest substitutional neighbors of an interstitial oxygen atom after jumping into a nearest-interstitial position. For fcc metals, $Z = 4$. For the frequency ν, we used the vibration frequency of the freely diffusing oxygen as obtained from Eq. (6): $\nu = 2.6 \times 10^{13}$ Hz. For the reaction constant k_{BO}^A we used the same value as for k_B^A.

The dissociation constant k_{BO}^D can be written as

$$k_{BO}^D = Z'\nu' \exp\left[\frac{-H_{BO}}{kT}\right] . \tag{9}$$

For an interstitial oxygen atom trapped at a substitutional B atom, the geometric factor for detrapping equals $Z' = \frac{3}{4}$. For the frequency, we used again the frequency of the free oxygen atom, $\nu' = 2.6 \times 10^{13}$ Hz. The dissociation enthalpy H_{BO} of the BO molecule is then left as the only free parameter in the two-step model. In the case that H_{BO} is stable, k_{BO}^D vanishes, and the two-step oxidation model approaches Wagner's model. A schematic potential-energy diagram of the internal-oxidation mechanism according to the two-step oxidation model is shown in Fig. 1.

III. EXPERIMENTAL DETAILS

A. Sample preparation

Slices of 1.5–3-mm thickness were cut from a 99.999%-pure silver single-crystal rod and polished mechanically and electrochemically. Before implantation, the samples were annealed at 1000 K for 20 min in a H_2 flow in order to remove possible electropolishing reagents.

The samples were implanted at room temperature in a nonchanneling direction in a vacuum better than 10^{-6} mbar. The indium atoms were implanted with an energy of 110 keV with a dose of 4×10^{15} atoms/cm^2 consisting almost entirely of stable ^{115}In and a very low dose of radioactive ^{111}In. For the ^{111m}Cd measurements, only ra-

dioactive ^{111m}Cd was implanted at 60-keV energy with a dose of less than 1×10^{11} atoms/cm^2.

After the implantation the samples were annealed at 723 K for 10 min in a H_2 flow in order to remove the implantation damage. The initial concentration profile of the indium (cadmium) is broadened by this annealing treatment by roughly a factor of 10, resulting in a Gaussian distribution of substitutional In atoms with its maximum at the surface and a full width at half maximum (FWHM) of 400 nm. The oxidation was performed in a quartz tube in which the pressure of the oxygen isotopes $^{18}O_2$ or $^{16}O_2$ could be regulated from 1 to 600 mbar. The oxidation temperature was regulated by an oven which was mounted around the quartz tube.

B. Time-differential perturbed angular correlation

In a TDPAC experiment one measures the perturbation of the angular correlation of two successively emitted γ quanta. This perturbation is caused by the hyperfine interaction of the nuclear electromagnetic moments of the intermediate level and the local electromagnetic field at the nucleus. Details of the method are described in detail by several authors.[11–13]

The TDPAC measurements were conducted at room temperature, using a setup consisting of four NaI(Tl) detectors. The detectors were positioned at relative angles $\theta_1=180°$ and $\theta_2=90°$ or 70.5°. Four coincidence spectra were recorded simultaneously, which were combined to form the ratio

$$R_{\text{expt}}(t)=2\frac{I(\theta_1,t)-I(\theta_2,t)}{I(\theta_1,t)+2I(\theta_2,t)}\ , \tag{10}$$

where $I(\theta,t)$ is the coincidence rate for a pair of detectors. In case of electric quadrupole interaction, the corresponding theoretical expression is approximated by[14]

$$R_{\text{theor}}(t)=\tfrac{2}{3}\sum_{\substack{k_1,k_2\\n,i}}[A_{k_1}(1)A_{k_2}(2)]_{\text{eff}}f_i[s^{\text{eff}}_{k_1k_2n}(\theta_1,t)-s^{\text{eff}}_{k_1k_2n}(\theta_2,t)]\cos[g_n(\eta_i)\nu_{Qi}t]\exp[-\delta_i g_n(\eta_i)\nu_{Qi}t]\ , \tag{11}$$

where f_i is the relative fraction of nuclei that experience a particular field i. The exponential function accounts for a Lorentzian frequency distribution with a mean value $g_n(\eta_i)\nu_{Qi}$ and a relative half-width δ_i. For the intermediate $\frac{5}{2}^+$ state of ^{111}Cd, the functions $g_n(\eta)$ are given by Gerdau[15] and the coefficients s^{eff} are extensively tabulated by Wegner.[14] The quadrupole frequency ν_Q is defined as $\nu_Q=eQV_{zz}/h$, where Q is the nuclear quadrupole moment, and V_{zz} is the z component of the diagonalized electric-field-gradient (EFG) tensor. The time-independent contribution to the perturbation function ($n=0$) is known as the hard-core value.

C. Nuclear-reaction analysis

The experimental details of nuclear-reaction analysis using the $^{18}O(p,\alpha)^{15}N$ reaction are described by Amsel.[16] This reaction was used for two types of experiments, i.e., oxygen depth profiling and channeling.

The oxygen depth profiles were measured by energy analysis of the emitted α particles. The energy of the incident proton beam was set to 840 keV, the upper limit of a region between 820 and 840 keV, where the energy dependence of the cross section is relatively weak. With the incident proton beam perpendicular to the sample surface, a depth interval of 1 μm can be probed. Three surface-barrier detectors, with an energy resolution of 12 keV and a total solid angle of 0.06 sr, were placed at backward angles. With this setup, a measuring time of 12 h is needed to achieve a sensitivity of 0.05 at. % in the determination of the ^{18}O concentration profile in silver.

During the channeling experiments the beam energy was 640 keV. The α-particle yield was measured in this case with a large surface-barrier detector ($\Omega=0.55$ sr), covered with a 12-μm-thick Hostaphan® foil. All elastically scattered protons were stopped in this foil, thus increasing the permissible beam intensity. Simultaneously the elastically scattered protons were monitored with a pinhole surface-barrier detector. Channeling profiles of the silver host atoms were obtained from the yield as a function of angle, within a narrow energy window on the spectrum of elastically scattered protons. This window corresponds to a depth region of approximately 0–250 nm. Because of the energy straggling caused by the Hostaphan® foil, the α-particle spectrum hardly contains depth information. Therefore, the channeling profiles of the oxygen atoms were obtained from the total α-particle yield.

In the analysis the experiments were compared to Monte Carlo simulations.[17] For the host atoms Rutherford backscattering (RBS) spectra were simulated and the same energy window as in the experiment was set to simulate the channeling profiles. The channeling profiles of the oxygen were simulated taking into account the oxygen depth profile as well as the energy-dependent cross section.[16] The simulation reproduces the actual energy loss, which is strongly reduced in a channeling direction. This has a particularly strong effect on the shape of the flux peak observed for (near-) interstitial impurities.

The top view of the setup used for oxygen lattice-site location is shown in Fig. 2. Both the channeling and the depth profiling measurements were done with the sample at room temperature.

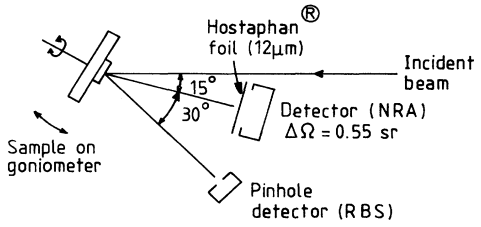

FIG. 2. Schematic top view of the experimental setup used for lattice-site location of oxygen 18.

IV. RESULTS

In Fig. 3 typical ^{111}In TDPAC spectra of silver single crystals implanted with stable indium to a dose of 4×10^{15} In atoms/cm^2 at 110 keV are shown after various annealing and oxidation treatments. The spectra were recorded along the ⟨110⟩ axes with the sample at room temperature. Figure 3(a) shows that a completely unperturbed spectrum is obtained after annealing the implanted crystal for 10 min at 723 K in a H_2 flow. By this annealing treatment most of the implantation damage has been removed and all indium atoms occupy substitutional sites.

A. Indium-oxygen 2*a* complex

Internal oxidation of the indium atoms was achieved by heating the crystal to 550 K in 100 mbar $^{18}O_2$. The spectra shown in Figs. 3(b) and 3(c) were obtained with two different samples which were oxidized for 1 and 10 min, respectively. Both spectra can be fitted assuming a broad distribution of electric quadrupole interactions, characterized by the parameters

$$\nu_Q = 50(3)\ \text{MHz},\quad \delta = 0.7(1),\quad \eta = 0.0(1)\ ,$$

with $f_{ox}=0.20(5)$ for the partly oxidized sample and $f_{ox}=1.00(5)$ for the completely oxidized sample. These values are somewhat different from the values given by Desimoni *et al.*[2] for a 1% In*Ag* foil oxidized at 573 K in open air. Uhrmacher *et al.*[3,6] again found slightly different values for a preoxidized 0.5% In*Ag* alloy after isochronal annealing in the temperature range 300–573 K. The alloy was preloaded with oxygen by rapid cooling of the foil in an oxygen-rich atmosphere. The ^{111}In TDPAC parameters as determined by these groups are collected in Table I. In spite of the differences, we think that all these measurements refer to the same type of indium-oxygen complexes, denoted the 2*a* complex.

We have determined the direction of the EFG by recording TDPAC spectra along different crystallographic directions. These spectra are shown in Fig. 4. The large hard-core value and the slow rise of $R(t)$ in the measurement with the detectors parallel to the ⟨100⟩ crystallographic directions is characteristic for a ⟨100⟩ direction of the principal axis of the EFG. Good fits are obtained by using the parameters of the 2*a* complex given above and by assuming an axial symmetric EFG with the principal axis pointing in a ⟨100⟩ direction. The hard-core values, which were the only free parameters in fitting the spectra, are given in Table II together with the hard-core values as expected from the tabulated coefficients s^{eff} for this geometry. The differences are only partly due to the finite solid angles of the detectors. An explanation might be that the principal axes of the EFG are slightly different for the different complexes.

The oxygen concentration profiles of these samples are shown in Fig. 5. In the analysis, no deconvolution of the

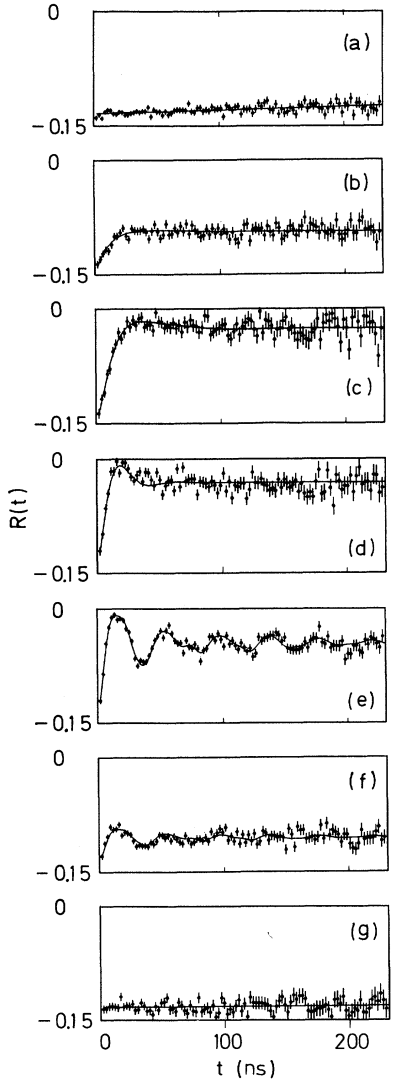

FIG. 3. ^{111}In TDPAC spectra of silver single crystals implanted with stable indium to a dose of 4×10^{15} atoms/cm^2 after various oxidation and annealing treatments. The spectra were recorded along ⟨100⟩ crystallographic directions: (a) annealed for 10 min at 723 K in H_2 flow, (b) as (a) and oxidized for 1 min at 550 K in 50 mbar $^{18}O_2$, (c) as (a) and oxidized for 10 min at 550 K in 300 mbar $^{18}O_2$, (d) as (c) and annealed for 10 min at 750 K in 400 mbar $^{18}O_2$, (e) as (d) and annealed for 10 min at 873 K in vacuum, (f) as (e) and annealed for 10 min at 1023 K in vacuum, and (g) as (f) and annealed for 10 min at 1043 K in vacuum.

TABLE I. ^{111}In-TDPAC parameters of indium-oxygen complexes in silver.

Site	ν_Q (MHz)	δ	η	f	Direction of EFG z axis	Oxid. or anneal temp. (K)	Ref.
2*a* complex	59(6)	0.3(1)	<0.02	1		300–600	3,6
	64(3)	0.4(1)	0.5(2)	1		573	2
	50(3)	0.7(1)	0.0(2)	1	⟨100⟩	550–600	present study
2*b* complex	95–120	0.4(1)	0.70(15)	1		575–1175	3,6
	118(4)	0.35(1)	0.75(5)	1		623–723	2
	90(3)	0.46(6)	0.8(2)	1	⟨100⟩	700–773	present study
In_2O_3 precipitates	116(2)	0.09(1)	0.69(4)	0.75(4)		775–1125	4
	157(3)	0.004(1)	0.29(2)	0.25(4)			
	118(3)	0.08(2)	0.75(2)	0.6(1)		723–1273	2
	156(3)	0.04(1)	0.22(2)	0.4(1)			
	111(1)	0.10(1)	0.8(1)	0.72(5)		873–1023	present study
	157(2)	0.03(1)	0.2(1)	0.28(5)			
Bulk In_2O_3	119(2)	0	0.69(5)	0.77(3)			22
	154(2)	0	0.00(5)	0.23(3)			

energy spectrum was applied since the depth resolution was much better than needed to monitor the smooth variations in the concentration profile. Since the oxidized fraction is known from the TDPAC spectra, the stoichiometry of the In-O complexes formed can be determined by measuring the oxygen dose and dividing this number by the oxidized indium dose. This ratio is found to be 1.8(2) for the partly oxidized sample and 2.0(1) for the completely oxidized sample. This means that each indium atom in the 2*a* complex has trapped two oxygen atoms. We may safely assume that these complexes consist of only one indium atom, because these 2*a* complexes are also formed in silver samples with very low indium concentrations even after very short oxidation. In that case the probability that the indium has agglomerated in clusters of at least two indium atoms is practically zero.[2,4] Thus, these complexes can be considered as isolated InO_2 molecules in a silver host.

Another important aspect of the depth profiling measurements is the shape of the oxygen profile. As expected, the oxygen profile of the fully oxidized sample resembles the indium profile, calculated using the known diffusion constant.[18] More interesting is the oxygen profile of the partly oxidized sample since it displays how the oxidation proceeds. Based on Wagner's model of internal oxidation,[8] one would expect a distinct oxidation front, i.e., a sharp boundary between the oxidized indium atoms near the surface and the nonoxidized indium atoms at deeper layers (in our case with a width of ~ 5 nm, according to an expression derived by Meijering and Druyvesteyn[19]). However, we observe a rather smooth oxygen profile, showing that the oxidized indium atoms are distributed over a few hundred nanometers. This demonstrates that the formation of InO_2 is not a simple one-step trapping process. The two-step oxidation model is in good agreement with experiment if one takes the dissociation enthalpy of the intermediate InO complex as $H_{InO}=0.60(5)$ eV. This is shown by the solid lines in Fig. 5. Comparing this value for the dissociation enthalpy with the oxygen migration enthalpy $E_O^m=0.48$ eV we can conclude that the In-O complex is only marginally stable. The depth profiles can be reproduced using Wagner's model only if we assume a trapping radius of $\frac{1}{30\,000}$ of a lattice constant. Such a small value has no physical meaning.

We have used the fully oxidized sample for a channel-

TABLE II. Experimental hard-core values of indium-oxygen complexes along different crystallographic directions. Also, the calculated hard-core values are given for an EFG with η and the x, y, and z axes as indicated.

Site	Hard-core values along ⟨100⟩	⟨110⟩	⟨111⟩	EFG in the calculation η	x	y	z
2*a*	0.41(1)	0.17(1)	0.12(1)				
	0.50	0	0	0			[001]
2*b*	0.45(1)	0.21(1)	0.21(1)				
	0.72	0	0	0.8	[100]	[010]	[001]

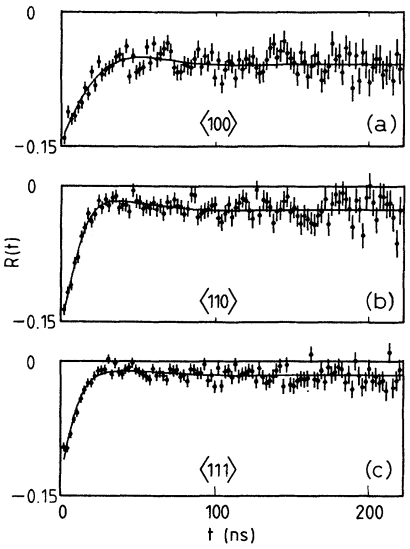

FIG. 4. ^{111}In TDPAC spectra of the 2*a* complexes recorded along different crystallographic directions as indicated.

ing experiment to locate the lattice site of the oxygen atoms in the 2*a* complexes. Angular scans through the major axes measured with the sample at room temperature are shown in Fig. 6. The damage produced by the analyzing beam (2 μC per point in an angular scan) was minimized by measuring at the angles near the string direction first and by taking a new beam spot after each scan. The pronounced flux peak in the ⟨110⟩ scan and the dips in the ⟨100⟩ and ⟨111⟩ scans are unquestionably the consequence of a near-octahedral interstitial site of the oxygen. The computer simulations gave a satisfactory correspondence with the experiment when all oxygen atoms are shifted 0.5(1) Å from the octahedral interstitial site in a ⟨111⟩ direction. In the simulations, a Debye temperature of $\Theta_D = 250$ K for the oxygen atoms was

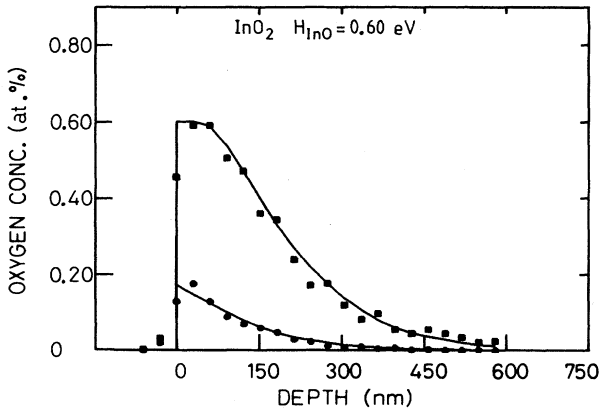

FIG. 5. Concentration profiles of the oxygen trapped at the 2*a* complexes of a 100(5)% and a 20(2)% oxidized sample. Solid lines are the results of a calculation using the two-step oxidation model.

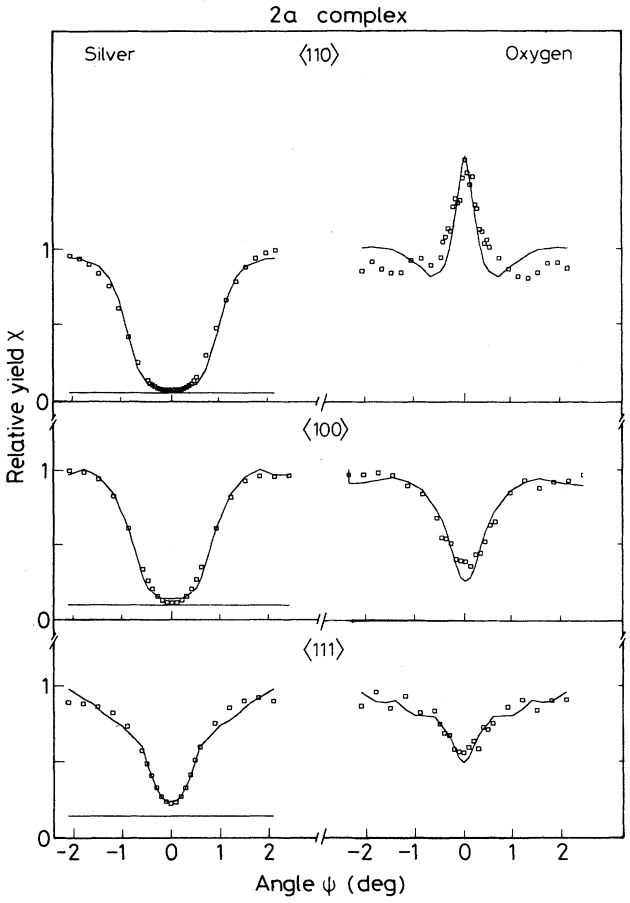

FIG. 6. Angular scans through the major axes of a single crystal with only 2*a* complexes. Simulations (solid lines) show that all the oxygen is trapped at near-octahedral intersitial sites.

assumed, corresponding with a rms vibrational amplitude in one dimension of 0.1 Å.

In Fig. 7, a possible arrangement of the InO_2 2*a* complex is shown that could explain both the TDPAC and the channeling measurements. A point-charge-model calculation gives for this configuration an EFG with the principal axis pointing in the [100] crystallographic direction and with an asymmetry parameter $\eta = 0.1$. Howev-

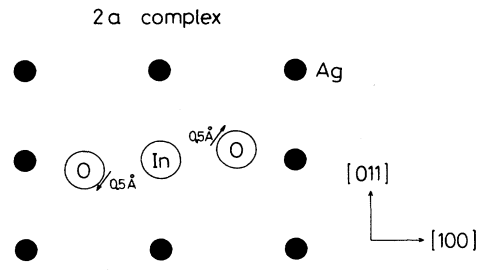

FIG. 7. Possible arrangement of the isolated 2*a* complex in the silver matrix.

er, there are several other configurations that can explain the measurements. For instance, a configuration is possible in which the oxygen atoms are at opposite sides but shifted in different ⟨111⟩ directions.

B. Indium-oxygen 2*b* complex

A third sample was prepared by implantation of 4×10^{15} indium-atoms/cm^2 and subsequent annealing at 723 K for 10 min in a H_2 flow. Complete oxidation of the indium in 2*a* complexes was achieved by oxidation for 10 min at 550 K in 300 mbar $^{18}O_2$. After subsequent annealing for 10 min at increasing temperatures in vacuum (or in 100 mbar $^{18}O_2$, which gives the same result), the quadrupole interaction parameters gradually change to the following values found for the temperature interval 700–750 K:

$$\nu_Q = 90(3)\ \text{MHz},\quad \delta = 0.46(6),\quad \eta = 0.8(2)\ .$$

These values are close to the values given in the literature for the so-called 2*b* complex. However, as in the case of the 2*a* complex, our value for the quadrupole frequency is somewhat low (cf. Table I).

Spectra taken at different crystallographic directions are shown in Fig. 8. For the least-squares fits of the perturbation function we assumed that the principal axis of the EFG lies along the [100] direction. The directions of the x and y axes were chosen parallel to [010] and [001] directions. The expected hard-core values for this symmetry are also tabulated in Table II. Although the trend is reproduced, there are appreciable differences between calculation and experiment, suggesting that the actual situation is more complicated.

The oxygen concentration profile of this sample, with only 2*b* complexes, proves to be identical to the oxygen profile of the completely oxidized sample with only 2*a* complexes (cf. Fig. 5). This implies that also for the 2*b* complexes two oxygen atoms are bound at each oxidized indium atom. The 2*b* complex is formed by annealing at 700 K even in very dilute systems,[2,4] indicating that the change of the EFG is due to a thermally activated change in the oxygen-indium geometry rather than an effect of clustering. Consequently, the 2*b* complexes are also isolated InO_2 molecules.

The results of channeling measurements for this sample are shown in Fig. 9. The angular scans through the major axes ⟨110⟩, ⟨100⟩, and ⟨111⟩ all show a dip in the string direction, which is a clear indication of a near-substitutional site for at least a considerable fraction of the trapped oxygen atoms. Channeling simulations show that several possibilities for the lattice site of the trapped oxygen can explain these measurements. The fits shown in Fig. 9 are obtained by taking a Debye temperature of $\Theta_D = 250$ K for the oxygen atoms and by assuming that 40% of the oxygen atoms are shifted 0.4(1) Å from the substitutional site in a ⟨110⟩ direction. The remaining 60% of the oxygen atoms give a random contribution, which implies that these atoms are neither in a near-substitutional site nor in a near-interstitial site. A possible configuration for the InO_2 2*b* complex with the oxygen atoms in near-substitutional sites is shown in Fig. 10. The point-charge model gives, for this arrangement, an EFG with an asymmetry parameter $\eta = 0.9$ with the x, y,

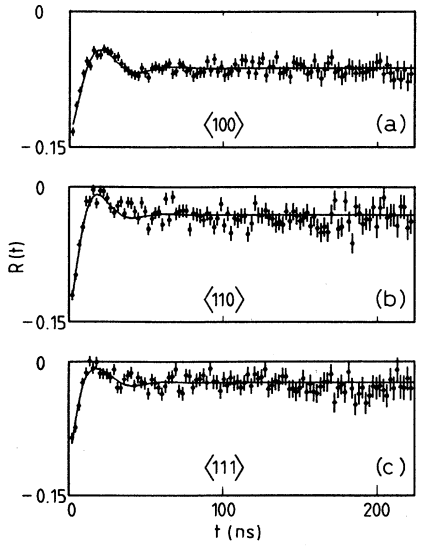

FIG. 8. ^{111}In TDPAC spectra of the 2*b* complexes recorded along different crystallographic directions as indicated.

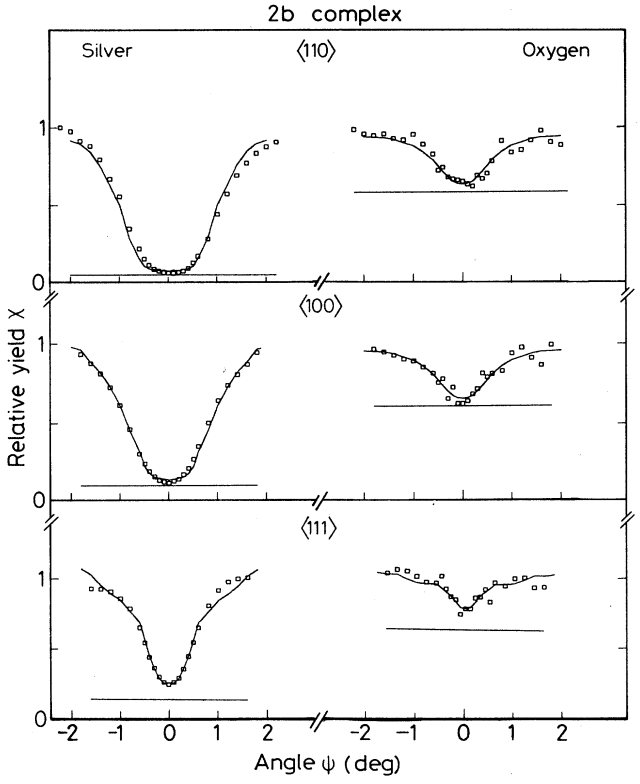

FIG. 9. Angular scans through the major axes of a single crystal with only 2*b* complexes. Simulations (solid lines) show that about 40% of the oxygen is trapped at near-substitutional sites.

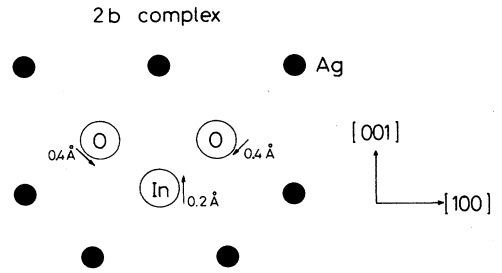

FIG. 10. Possible arrangement of the isolated 2*b* complex in the silver matrix.

and *z* axes pointing in different ⟨100⟩ directions. This agrees very well with the TDPAC measurements. We may conclude that due to the anneal at 700 K the position of a large fraction of the oxygen atoms has changed from a near-interstitial site in the 2*a* complexes to a near-substitutional site in the 2*b* complexes. This change may be caused by the trapping of thermally activated vacancies at the 2*a* complexes. If a vacancy is trapped by a 2*a* complex, space is created for the relaxation of the near-interstitial oxygen atoms into near-substitutional sites. In order to see if this picture is correct, we used the two-step oxidation model to simulate the trapping of two vacancies at isolated InO_2 complexes. We assumed that the vacancy concentration at the surface is maintained during annealing time and equals the equilibrium bulk vacancy concentration[13] $C_V^s \simeq \exp(-H_V^F/kT)$, with $H_V^F = 1.10$ eV. From the known vacancy jumping frequency[20] $\nu = 2.16 \times 10^{12}$ Hz and vacancy migration energy[21] $E_V^m = 0.62$ eV the input parameters [cf. Eqs. (6), (8), and (9)] can be calculated. The dissociation constant $k_{(\mathrm{InO})V}$ was assumed to be zero. According to the calculations, the time needed to associate all InO_2 complexes with two thermally created vacancies is 35 min at 700 K and 10 min at 750 K. Experimentally, the $2a \rightarrow 2b$ transition occurs in about 10 min at 700 K. In view of the crude assumptions made in the calculation, the agreement is reasonable.

C. Precipitation of the 2*b* complexes

A fourth sample, prepared exactly in the same way as the previous sample containing 2*b* complexes only, was annealed at 773 K for 10 min in vacuum. The TDPAC spectrum taken after this anneal shows no significant changes. However, after annealing at 873 K the spectrum changed drastically [see Fig. 3(e)], showing two well-defined quadrupole interactions, with

$$\nu_{Q_1} = 111(1)\ \text{MHz},\quad \delta_1 = 0.10(1),\quad \eta_1 = 0.8(1)\ ,$$

$$\nu_{Q_2} = 157(2)\ \text{MHz},\quad \delta_2 = 0.03(1),\quad \eta_2 = 0.2(1)\ .$$

The ratio $f_1 : f_2$ of the fractions having these interactions is about 3:1. These parameters match very well with TDPAC measurements on bulk In_2O_3, where the two quadrupole interactions correspond to the two different coordinations of six oxygen atoms around an indium atom.[22]

Additional NRA experiments were performed on a fifth sample that was oxidized at 550 K and subsequently annealed in vacuum at 873 K. The corresponding PAC spectra and the depth profile after oxidation at 550 K were identical with those shown earlier. The anneal at 873 K did not lead to a change in the depth profile, apart from a slight enrichment at the surface. However, the $[^{18}O]/[In]$ ratio changed from 2.0(1) to 1.45(10). This obviously means that the 2*b* complexes agglomerated into In_2O_3 precipitates while the excess ^{18}O diffused out of the crystal. This type of precipitation has also been observed in In*Ag* alloys by Wodniecki and Wodniecka[4] and Desimoni *et al.*,[2] who found a strong dependence of the growth of the precipitates on the indium concentration.

The fact that the depth profile does not change appreciably during annealing at 873 K implies that precipitation occurs locally, without long-range diffusion. The most straightforward explanation of this phenomenon is that individual InO_2 complexes become mobile at this temperature and cluster into precipitates. The essential point in this description is that the constituent atoms of the complex perform a correlated diffusion process.

An alternative explanation would be that InO_2 molecules break up and that the atoms move individually through the lattice to already existing precipitates. The problem with this picture is that, at least in the initial stage of the precipitation, the surface is expected to be the dominant sink for the diffusing ^{18}O atoms. This will result in a large out-diffusion of ^{18}O because no stable surface adsorption sites are available at this temperature.[23]

After annealing at 1023 K, a large part of the In_2O_3 precipitates have dissociated [see Fig. 3(f)]. They are completely dissociated at 1043 K, resulting in the unperturbed spectrum shown in Fig. 3(g).

In Fig. 11 the TDPAC measurements on internally oxidized silver single crystals are summarized by displaying the relative fractions of the various components and their quadrupole frequencies as a function of annealing temperature.

D. Internal oxidation of Cd in silver

In the interpretation of the ^{111}In TDPAC spectra, the following argument may be important. ^{111}In decays by electron capture to a short-lived excited state of ^{111}Cd, which subsequently decays by the γ-γ cascade used for the measurement of the TDPAC. This means that the hyperfine interactions are measured on cadmium-oxygen complexes whereas the geometrical structure, at least initially, is determined by the formation of the indium-oxygen complexes. In order to see if the cadmium-oxygen complexes formed by internal oxidation of indium have the same geometrical structure as the cadmium-oxygen complexes formed by internal oxidation of cadmium, we have performed internal oxidation experiments on cadmium implanted in silver. In Fig. 12, ^{111}Cd TDPAC spectra of a silver single crystal implanted with only ^{111m}Cd at 60 keV to a very low dose, below 1×10^{11} atoms/cm^2, are shown. After annealing at 723 K for 10 min in H_2, various oxidation treatments were given. Fig-

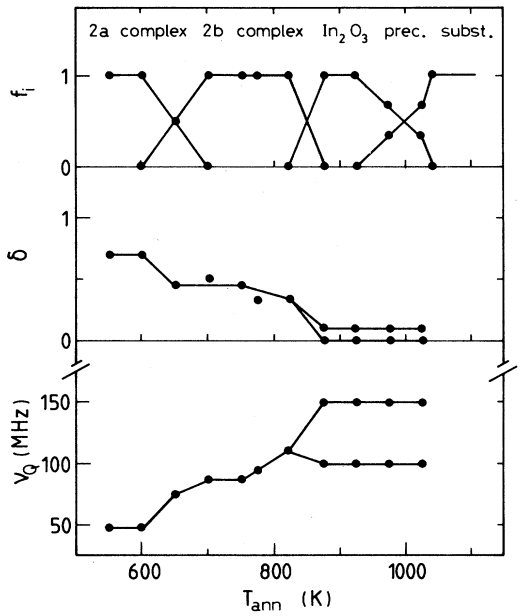

FIG. 11. ^{111}In TDPAC parameters ν_Q, δ, and relative fractions f_i as a function of the annealing temperature, as derived from spectra partly shown in Fig. 3.

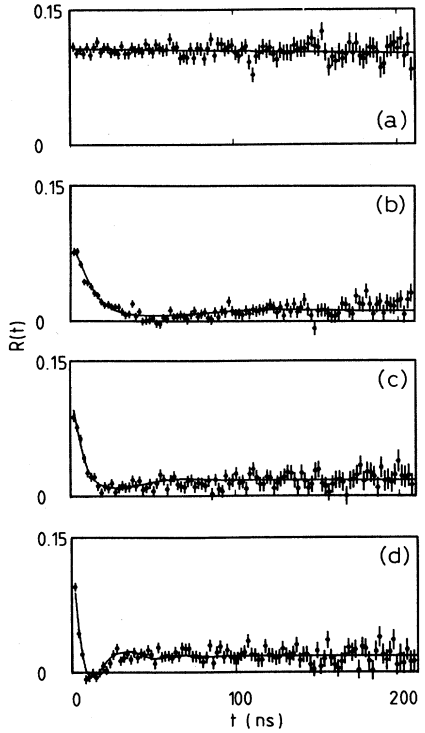

FIG. 12. ^{111m}Cd TDPAC spectra of cadmium implanted with 60 keV to a dose below 1×10^{11} atoms/cm^2 in a single crystal after various annealing and oxidation treatments: (a) annealed for 10 min at 723 K in 1 atm H_2, (b) as (a) and oxidized for 5 min at 650 K in 600 mbar O_2, (c) as (a) and oxidized for 5 min at 750 K in 600 mbar O_2, and (d) as (a) and oxidized for 5 min at 850 K in 600 mbar O_2.

ure 12(a) shows the unperturbed spectrum which was recorded just after the hydrogen anneal. Figure 12(b) shows the spectrum obtained after oxidation at 650 K for 5 min in 600 mbar O_2. The quadrupole interaction is given by the parameters

$$\nu_Q=49(2)\ \text{MHz},\quad \delta=0.6(1),\quad \eta=0.0(2)\ .$$

These values are equal, within the accuracy of the measurement, to the parameters of the indium-oxygen 2*a* complex.

The oxidation at 750 K for 5 min in 600 mbar O_2 resulted in the spectrum shown in Fig. 12(c), with fitted parameters

$$\nu_Q=83(6)\ \text{MHz},\quad \delta=0.6(1),\quad \eta=0.3(3)\ .$$

After oxidation at 850 K for 5 min in 600 mbar O_2, the TDPAC spectrum shown in Fig. 12(d) reflects much higher quadrupole frequencies,

$$\nu_Q=171(6)\ \text{MHz},\quad \delta=0.31(5),\quad \eta=0.4(1)\ .$$

Summarizing these experiments, oxidation at 650 K of very dilute cadmium in silver results in a ^{111}Cd TDPAC spectrum which greatly resembles the ^{111}In TDPAC spectra of 2*a* complexes formed by the internal oxidation of dilute indium in silver. This indicates that cadmium-oxygen complexes formed at these temperatures have the same geometrical structure as the indium-oxygen 2*a* complexes. At higher oxidation temperatures, the spectra obtained from internally oxidized cadmium differ from the ^{111}In TDPAC spectra of the indium-oxygen 2*b* complexes observed after internal oxidation of very dilute indium in silver.[2,4] This means that at these temperatures the geometrical structure of the isolated cadmium-oxygen complexes differs from the structure of indium-oxygen 2*b* complexes.

V. DISCUSSION

Several authors have discussed the appearance of the broad frequency distributions in the TDPAC spectra for the 2*a* and 2*b* complexes. One interpretation has been that these broad distributions are due to *aftereffects*, i.e., a time-dependent perturbation of the angular correlation due to short-lived holes in the valence band caused by the electron-capture decay of the ^{111}In nucleus just before the cadmium γ-γ cascade. However, this possibility can be ruled out by the TDPAC studies of Massolo *et al.*[22] on aftereffects in In_2O_3 precipitates in a silver matrix. They observed aftereffects only in large In_2O_3 precipitates. Therefore, it is very unlikely that these processes are important in the small InO_2 molecules that are closely surrounded by the conduction electrons of the metallic host.

Another explanation might be that the broad distribution is caused by fluctuations in the nearest environment of the In (Cd) atoms, caused, for instance, by local hopping of the O atoms. Since we have observed no change in the spectra obtained from a sample with only 2*a* complexes during variation of the measurement temperature in the region $T_M=77-573$ K, this possibility is unlikely too. Moreover, the hard-core values obtained are in good

agreement with a static distribution of quadrupole frequencies.

Consequently, we have to assume that the broad frequency distribution is due to differences in the geometrical structure of the 2*a* and 2*b* complexes. The geometrical structure will determine the amount of *p* character of the valence electrons participating in the In—O bonds and the orientation of these bonds. It is to be expected that the *p*-orbital contribution of these valence electrons dominates the EFG at the In (Cd) site. Indeed, recent TDPAC measurements on a number of oxidic compounds in which ^{111}In was incorporated show that the quadrupole interaction is very much dependent on the local geometry.[24] The strong correlation with the In-O distance is much less convincing than was claimed earlier.[25] Such a correlation can be understood in a simple ionic picture in which the contribution of the O^{2-} ions to the EFG is amplified by a distance-dependent Sternheimer antishielding factor. In any case, one expects a sensitive dependence of the EFG on the local structure of the InO_2 complex.

One can speculate about the mechanism that leads to the variations in the local structure of the InO_2 complexes. The distance between the octahedral interstitial site and the substitutional site in silver is 2.04 Å. This is practically equal to the Ag—O bond length in Ag_2O and AgO, whereas the In—O bond length in In_2O_3 is 2.2 Å. Consequently, one expects the oxygen atoms to shift from the octahedral position, and this is indeed observed in our channeling measurements. In fact, the In—O bond lengths derived from the tentative configurations proposed for the 2*a* complex (Fig. 7) and the 2*b* complex (Fig. 10) are even larger than in bulk In_2O_3: 2.4 and 2.5 Å, respectively. Consequently, the InO_2 molecules will introduce local strain in the silver lattice. It seems that this strain is responsible for the large number of slightly different configurations. However, our understanding of this problem is still in a very preliminary stage.

VI. CONCLUSIONS

Internal oxidation of dilute indium in silver at 550 K results in the formation of isolated indium-oxygen 2*a* complexes. The EFG of these complexes is axially symmetric with the principal axis pointing in a ⟨100⟩ direction. The trapped oxygen is located near octahedral interstitial sites. By subsequent annealing above 700 K, the 2*a* complexes change into 2*b* complexes. The main axis of the EFG of the 2*b* complexes also points in a ⟨100⟩ direction, but the asymmetry parameter has changed to $\eta = 0.8(2)$. Now, 40% of the oxygen is located in near-substitutional sites, indicating that the transformation of the 2*a* complexes into 2*b* complexes is probably due to trapping of thermal vacancies. By annealing above 873 K, the 2*b* complexes form In_2O_3 precipitates, which means that isolated 2*b* complexes are mobile at these temperatures. Oxidation below 700 K of very dilute cadmium in silver results in the formation of cadmium-oxygen complexes with the characteristics of the indium-oxygen 2*a* complexes.

ACKNOWLEDGMENTS

The authors would like to thank F. Pleiter, M. Deicher, and H. Haas for help and discussions during various stages of the experiments. This work was supported in part by the Stichting voor Fundamenteel Onderzoek der Materie (FOM) with financial support from the Nederlandse Organisatie voor Zuiver Wetenschappelijk Onderzoek (ZWO).

[1] A. F. Pasquevich, A. G. Bibiloni, C. P. Massolo, and F. H. Sánchez, Phys. Lett. **82A**, 34 (1981).

[2] J. Desimoni, A. G. Bibiloni, L. Mendoza-Zélis, A. F. Pasquevich, F. H. Sánchez, and A. López-García, Phys. Rev. B **28**, 5739 (1983).

[3] W. Bolse, P. Wodniecki, H. Schröder, M. Uhrmacher, and K. P. Lieb, Phys. Lett. **93A**, 429 (1983); H. Schröder, W. Bolse, P. Wodniecki, M. Uhrmacher, and K. P. Lieb, Nucl. Instrum. Methods B **2**, 706 (1984).

[4] P. Wodniecki and B. Wodniecka, Hyperfine Interact. **12**, 95 (1982).

[5] A. F. Pasquevich, A. F. Sánchez, A. G. Bibiloni, J. Desimoni, and A. López-García, Phys. Rev. B **27**, 963 (1983).

[6] H. Schröder, W. Bolse, M. Uhrmacher, P. Wodniecka, and K. P. Lieb, Z. Phys. B **65**, 193 (1986).

[7] D. Wegner, M. Urhmacher, and K. P. Lieb, Z. Phys. B **68**, 461 (1987).

[8] C. Wagner, Z. Elektrochem. **63**, 772 (1959).

[9] W. Segeth, D. O. Boerma, L. Niesen, J. R. Heringa, and A. van Veen, Z. Phys. B **73**, 43 (1988).

[10] W. Eichenhauer and G. Müller, Z. Metallk. **53**, 321 (1962); **53**, 700 (1962).

[11] H. Frauenfelder and R. M. Steffen, in *Alpha-, Beta-, and Gamma-Ray Spectroscopy,* edited by K. Siegbahn (North-Holland, Amsterdam, 1965), Chap. 19(A).

[12] R. M. Steffen and K. Adler, in *The Electromagnetic Interaction in Nuclear Spectroscopy,* edited by W. D. Hamilton (North-Holland, Amsterdam, 1975), Chap. 12.

[13] E. Recknagel, G. Schatz, and Th. Wichert, in *Hyperfine Interactions of Radioactive Nuclei,* Vol. 31 of *Topics in Current Physics,* edited by J. Christiansen (Springer, Berlin, 1983), p. 133.

[14] D. Wegner, Hyperfine Interact. **23**, 179 (1985).

[15] E. Gerdau, J. Wolff, H. Winkler, and J. Braunsfurth, Proc. R. Soc. London, Ser. A **311**, 197 (1969).

[16] G. Amsel and D. Samuel, Anal. Chem. **39**, 1689 (1967).

[17] P. J. M. Smulders and D. O. Boerma, Nucl. Instrum. Methods B **29**, 471 (1987).

[18] *CRC Handbook of Chemistry and Physics,* edited by R. C. Weast (CRC, Boca Raton, 1986).

[19] J. L. Meijering and M. J. Druyvesteyn, Philips Res. Rep. **2**, 81 (1947); **2**, 260 (1947).

[20] A. Seeger and H. Mehrer, in *Vacancies and Interstitials in Metals,* edited by A. Seeger, D. Schumacher, W. Schilling, and J. Diehl (North-Holland, Amsterdam, 1970), p. 1.

[21] R. W. Balluffi, in *Properties of Atomic Defects in Metals,* edited by N. L. Peterson and R. W. Siegel (North-Holland, Amsterdam, 1978), p. 240.

[22]C. P. Massolo, J. Desimoni, A. G. Bibiloni, L. A. Mendoza-Zélis, F. H. Sánchez, A. F. Pasquevich, and A. R. López-García, Hyperfine Interact. **30**, 1 (1986).
[23]W. Segeth, J. H. Wijngaard, and G. A. Sawatzky, Surf. Sci. **194**, 615 (1988).
[24]W. Bolse (private communication).
[25]W. Bolse, M. Uhrmacher, and J. Kesten, Hyperfine Interact. **34/35**, 931 (1987).